ELSEVIER

Polymer 43 (2002) 7279–7288

polymer

www.elsevier.com/locate/polymer

Surface modification of polyimide films via plasma polymerization and deposition of allylpentafluorobenzene

Y. Zhang[a], E.T. Kang[a,*], K.G. Neoh[a], W. Huang[b], A.C.H. Huan[c], H. Zhang[d], R.N. Lamb[d]

[a]*Department of Chemical Engineering, National University of Singapore, Kent Ridge, Singapore, Singapore 119260*
[b]*Institute of Advanced Materials and Technology, Fudan University, 220 Handan Road, Shanghai 200433, People's Republic of China*
[c]*Institute of Materials Research and Engineering (IMRE), National University of Singapore, 3 Research Link, Singapore, Singapore 117602*
[d]*School of Chemistry, University of New South Wales, Sydney NSW 2052, Australia*

Received 13 May 2002; received in revised form 13 September 2002; accepted 4 October 2002

Abstract

Plasma polymerization of allylpentafluorobenzene (APFB) on the plasma-pretreated polyimide (PI) films was carried out. The fluorinated aromatic groups of the plasma-polymerized APFB (pp-APFB) could be preserved, to a large extent, by controlling the glow discharge parameters. The effect of the glow discharge parameters, including the type of the carrier gas and the input RF power, on the surface composition and chemical structure of the pp-APFB films were studied by X-ray photoelectron spectroscopy, Fourier transform infrared spectroscopy, and time-of-flight secondary ion mass spectrometry. The surface topography of the APFB plasma-polymerized PI (pp-APFB-PI) films was studied by atomic force microscopy. For plasma polymerization carried out at a high RF power and using argon as the carrier gas, an ultra-hydrophobic pp-APFB-PI surface was also obtained. The ultra-hydrophobic surface exhibited advancing/receding water contact angles (θ_A/θ_R) of 174°/135°. The effectiveness of the carrier gas in defluorinating the pp-APFB films followed the order of $O_2 > N_2 > H_2 >$ Ar. Thus, the role of the carrier gas in improving the surface hydrophobicity of the resulting pp-APFB-PI films followed the order of $O_2 < N_2 < H_2 <$ Ar. The adhesion of the pp-APFB layer to the PI substrate was investigated via solvent extraction and the Scotch® tape adhesion test.

Keywords: Polyimide; Allylpentafluorobenzene; Ultra-hydrophobic

1. Introduction

Poly(pyromellitic dianhydride-*co*-4,4′-oxydianiline) (PMDA-ODA)-based polyimide (PI) is one of the most widely used polymers in the microelectronics industry because of its excellent mechanical, thermal and dielectric properties. However, the relatively high dielectric constant (ε) of about 3.5 has limited its use in the ultra-large scale integration (ULSI) technology, where the requirement of the dielectric constant is <2.8 [1,2]. Furthermore, the moisture absorption (up to about 3 wt%) characteristic of the PI film can give rise to a further increase in its dielectric constant and decrease in its adhesion reliability to other substrates. On the other hand, fluoropolymers, such as poly(tetrafluoroethylene) (PTFE), have very low moisture uptake property and are among the materials with the lowest dielectric constants [3]. However, the poor adhesion characteristics of the fluoropolymers have limited their wide-spread applications in the microelectronics industry. The combination of the complementary physicochemical properties of PI and the fluoropolymers is, thus, of great interest to the microelectronics industry. A most widely used approach is to incorporate the fluorine-containing groups into the PI molecular chain to produce a new family of polyimides, viz. the fluorinated polyimides (FPIs) [4]. Other approaches have included the preparation of composite film via physical bonding. The commercial product under the trade mark of Kapton® FN, manufactured by DuPont Chem. Co., involves the bonding of a thin fluoropolymer layer to the PI surface. Surface fluorination of PI films via CF_4 gas plasma treatment has also been investigated [5–7]. A more recent effort has involved the thermal imidization of the poly(amic acid) precursors of PI on the glycidyl methacrylate graft-copolymerized PTFE film, followed by delamination to give rise to a PTFE-bonded PI film [8]. In addition, a number of excellent studies dealing with the plasma polymerization of

* Corresponding author. Tel.: +65-6874-2189; fax: +65-6779-1936.
E-mail address: cheket@nus.edu.sg (E.T. Kang).

0032-3861/02/$ - see front matter
PII: S0032-3861(02)00711-5

fluorine-containing monomers to produce fluoropolymer films with ultra-hydrophobic property and low dielectric constant have appeared recently [9–13]. Fluoromonomers, including perfluoroallylbezene [9], pentafluorostyrene [10], 1*H*,1*H*,2*H*-perfluoro-1-decene [11], 1*H*,1*H*,2*H*,2*H*-heptadecafluoro-decyl acrylate [12], and 2,2,3,3,4,4,4-heptafluorobutyl acrylate [13] have been employed. On the other hand, plasma polymerization of fluorine-containing monomers on PI substrates, the adhesion of the plasma-deposited fluoropolymers with the substrates, and the preservation of the molecular structure in the resulting fluoropolymer films have yet to be studied in detail.

In the present work, allylpentafluorobenzene (APFB) is plasma-polymerized and deposited on the Ar plasma-pretreated PI surface (the pp-APFB-PI surface). The APFB molecule contains a reactive allyl group and a stable fluorinated aromatic ring. With the proper choice of the glow discharge conditions, polymerization is expected to proceed mainly via the allyl groups, with the preservation of a high proportion of the fluorinated aromatic groups. A highly fluorinated and hydrophobic film can thus be deposited. Four types of carrier gases, viz. Ar, H_2, N_2 and O_2, are explored. The effects of the glow discharge parameters on the surface composition and topography of the pp-APFB-PI surfaces are characterized by X-ray photoelectron spectroscopy (XPS), Fourier transform infrared (FTIR) spectroscopy, and time-of-flight secondary ion mass spectrometry (ToF-SIMS). The extent of interaction of the pp-APFB films with the PI substrates was evaluated by solvent extraction and the Scotch® tape adhesion test.

2. Experimental

2.1. Materials

The polyimide (PI) film used in this study was obtained from the DuPont Chemical Co. as Kapton® HN in rolls of 40 mm in width and 75 μm in thickness. The surfaces of the PI films were cleaned with acetone in an ultrasonic water bath for 20 min and then dried at 80 °C under reduced pressure before use. The monomer, allylpentafluorobenzene (APFB), used for plasma polymerization was obtained from the Aldrich Chemical Co. of Milwaukee, WI, USA. The chemical structure of APFB monomer is shown below:

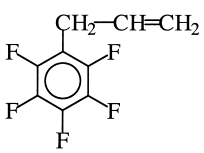

APFB

2.2. Plasma polymerization of APFB: the pp-APFB-film

The plasma polymerization apparatus was manufactured by Samco International of Kyoto, Japan (Model Samco BP-1). The physical geometry of the system had been described in detail previously [14,15]. The APFB monomer was introduced into the deposition chamber by the carrier gas from a thermostated monomer reservoir. The monomer–carrier gas mixture was allowed to flow into the reactor evenly from a distributor in the upper electrode. The carrier gases used included Ar, H_2, N_2, and O_2. A carrier gas flow rate of 20 standard cubic centimetre per min (sccm) and a monomer temperature of 25 °C were used throughout this work. The actual flow rates of the APFB monomer in the respective carrier gases were determined to be about 2×10^{-2}, 4×10^{-2}, 3×10^{-2}, and 1×10^{-2} sccm by experimentally measuring the time required for each carrier gas stream to evaporate a fixed amount of the liquid monomer. The glow discharge was ignited after impedance matching at a predetermined pressure of 0.6 Torr in all cases. The plasma-polymerized APFB film was obtained after a fixed deposition time of 40 s (for the PI surface) or 3 min (for the KBr pellet surface). In order to improve the interaction between the pp-APFB layer and the PI substrate, each PI film was pretreated with the respective carrier gas plasma [16] at a power of 20 W for 20 s prior to the plasma polymerization and deposition.

2.3. Surface characterization

The chemical compositions of the pristine and the APFB plasma-polymerized PI surfaces were determined by XPS. The XPS measurements were made on the AXIS HSi spectrometer (Kratos Analytical Ltd, England) with a monochromatized Al K_α X-ray source (1486.6 eV photons) at a constant dwell time of 100 ms and a pass energy of 40 eV. The anode voltage and current were set at 15 kV and 10 mA, respectively. The pressure in the analysis chamber was maintained at 5×10^{-8} Torr or lower during each measurement. The PI substrates with the deposited pp-APFB films were mounted on the sample stubs by means of double-sided adhesive tapes. The core-level signals were obtained at a photoelectron take-off angle (with respect to the sample surface) of 90°. All binding energies (BEs) were referenced to the C 1s neutral carbon peak at 284.6 eV. In curve fitting, the line width (full width at half maximum, or FWHM) for the Gaussian peaks was maintained constant for all components in a particular spectrum. Surface elemental stoichiometries were determined from peak-area ratios, after correcting with the experimentally determined sensitivity factors, and were reliable to ±5%. The elemental sensitivity factors were determined using stable binary compounds of well-established stoichiometries.

ToF-SIMS was also used for the surface analysis of the pp-APFB-PI films. The ToF-SIMS analysis was carried out on an ION-TOF SIMS IV instrument (ION-TOF, GmbH, Germany). The primary ion beam (10 keV Ar^+) with a spot size of ~50 μm was rastered over an area of 500 × 500 μm^2 while keeping the total dose under 10^{13} ions/cm^2. The

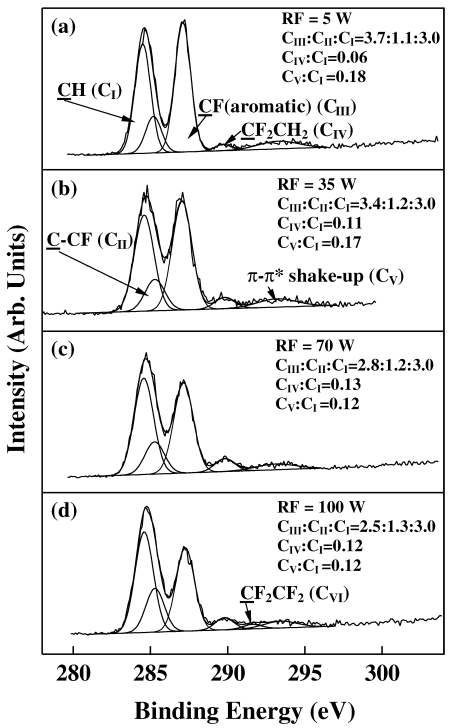

Fig. 1. C 1s core-level spectra of the plasma-polymerized APFB on PI surfaces at RF powers of (a) 5 W, (b) 35 W, (c) 70 W, and (d) 100 W, using Ar as the carrier gas.

pressure in the analysis chamber was maintained at 1×10^{-9} Torr or lower during each measurement. To reduce the charging effect, an electron flood gun was used for the charge neutralization. The calibration of the mass spectra was based on the built-in mass library.

2.4. FTIR spectroscopy

The pp-APFB samples for the FTIR spectroscopy measurements were obtained by depositing the plasma-polymerized APFB film directly on the surface of a freshly pressed KBr disc. The spectra were recorded in air on a Bio-Rad FT-IR, Model 400, spectrophotometer. Each spectrum was collected by cumulating 30 scans at a resolution of 8 cm^{-1}.

2.5. Water contact angle measurements

Receding and advancing water contact angles (θ_R and θ_A, respectively) on the pristine PI, the PTFE, the Kapton FN®, and the pp-APFB-PI (from Ar carrier gas) surfaces were measured in an automated contact angle goniometer, Model RHI 2001, of Ramé-Hart, Inc., New Jersey, USA, with the digital imaging software. Mathematical analysis of the true drop profile was achieved by fitting a fifth order polynomial.

Static water contact angles on the other pp-APFB-PI surfaces were measured by the sessile drop method at 25 °C and 65% relative humidity using a contact angle goniometers (Model 100-00-(230)) manufactured also by the Rame-Hart, Inc. The telescope with a magnification power of 23 × was equipped with a protractor of 1° graduation. For each contact angle reported, 10 readings from different parts of the film surface were averaged.

2.6. Characterization of the film thickness and surface morphology

The surface morphologies of the pp-APFB-PI films were studied by atomic force microscopy (AFM), using a Nanoscope IIIa AFM from the Digital Instruments Inc. In each case, an area of 5 μm × 5 μm was scanned using the tapping mode. The drive frequency was 330 ± 50 kHz, and the voltage was between 3.0 and 4.0 V. The drive amplitude was about 300 mV and the scan rate was 0.5–1.0 Hz. The scan angle was 0°. An arithmetic mean of the surface roughness (R_a) was calculated from the roughness profile determined by AFM. The thickness of the pp-APFB layer on PI was determined using an Alpha-STEP 500 Surface Profiler of KLA-Tencor Co., San Jose, CA from the pp-APFB film deposited simultaneous on a Si(100) single crystal wafer surface.

3. Results and discussion

3.1. Surface compositions of the plasma-polymerized APFB on the plasma-pretreated PI films (the pp-APFB-PI films)

Earlier studies have shown that the glow discharge parameters, such as the input RF power, the type of the carrier gas, the system pressure, and the flow rate of the carrier gas, can greatly affect the chemical structure and surface composition of the deposited polymer [15–18]. In the present work, the effects of the first two parameters on the properties of the resulting pp-APFB-PI films are emphasized. The system pressure and the carrier gas flow rate are kept constant at 0.6 Torr and 20 sccm, respectively. The abbreviations, pp-APFB-PI (Ar), pp-APFB-PI (H_2), pp-APFB-PI (N_2), and pp-APFB-PI (O_2), denote the plasma-polymerized APFB on PI films using Ar, H_2, N_2, and O_2, respectively, as the carrier gas.

Fig. 1 shows the respective C 1s core-level spectra of the pp-APFB-PI (Ar) surfaces prepared under the input RF powers of 5 W (Fig. 1(a)), 35 W (Fig. 1(b)), 70 W (Fig. 1(c)), and 100 W (Fig. 1(d)). In each case, plasma polymerization has resulted in the coverage of the PI film by the pp-APFB layer to a thickness beyond the probing depth of the XPS technique (~7.5 nm in an organic matrix [19]), as the nitrogen signal (at the BE of 400.6 eV [16]) from the underlying PI substrate is no longer discernible. The actual thickness values of the pp-APFB films, as determined using a surface profiler from the corresponding pp-APFB films deposited concurrently on the Si(100) wafer surfaces (see Section 2), are about 1.2, 2.0, 2.9 and 2.6 μm, respectively. The C 1s core-level spectra of the pp-APFB-PI

Table 1
Surface composition of the pp-APFB-PI films prepared using different carrier gases and different RF powers

Input RF power (W)	pp-APFB-PI (Ar)		pp-APFB-PI (H_2)		pp-APFB-PI (N_2)			pp-APFB-PI (O_2)	
	[F]/[C]	[O]/[C]	[F]/[C]	[O]/[C]	[F]/[C]	[O]/[C]	[N]/[C]	[F]/[C]	[O]/[C]
5	0.53	0.01	0.52	0.05	0.52	0.04	0.01	0.41	0.22
35	0.51	0.02	0.51	0.04	0.44	0.06	0.06	0.35	0.27
70	0.50	0.02	0.50	0.03	0.44	0.08	0.11	0.30	0.32
100	0.50	0.04	0.45	0.04	0.43	0.04	0.07	0.29	0.30
150	0.50	0.03	0.43	0.05	0.44	0.04	0.06	0.27	0.27

Note: the APFB molecule has a theoretical [F]/[C] ratio of 0.56 and an [O]/[C] ratio of 0.

(Ar) films can be curved-fitted with five peak components, having binding energies (BE's) at 284.6 eV for the *C*–H species (C_I), at 285.2 eV for the *C*–CF species (C_{II}), at 287.2 eV for the *C*F species (C_{III}), at 289.8 eV for the *C*F_2CH_2 species (C_{IV}), and at 293.2 eV for the $\pi-\pi^*$ shake-up satellite of the aromatic ring (C_V) [10,20]. No appreciable amount of the *C*F_3 species was detected at the BE of 294 eV. This fact is further confirmed by the absence of an appreciable intensity of the *C*F_3 fragment in the ToF-SIMS spectra (see blow).

Both the molar ratio of the *C*F/*C*–CF/*C*–H ($C_{III}/C_{II}/C_I$) species and the intensity ratio of the shake-up satellite to the *C*–H peak component (C_V/C_I) decrease with the input RF power. On the other hand, the amount of the *C*F_2CH_2 species formed (expressed as the C_{IV}/C_I ratio) during the plasma polymerization process increases with the input RF power. The variation in composition of the pp-APFB-PI (Ar) surfaces with the input RF power is probably attributable to the different bond scission mechanisms in the plasma polymerization process. Taking into consideration the difference in dissociation energies for the various chemical bonds, including the C=C, C–C, C–C (aromatic), C–H, and C–F bonds, different input RF powers will give rise to different patterns of bond scission in the APFB monomer, and hence different chemical structure of the plasma-deposited films. At low input RF power, excitation occurs mainly at the carbon–carbon π bond of the APFB molecule, which has the lowest bond energy [21]. Under this condition, molecular rearrangement of the excited states results predominantly in a plasma polymer having similar chain structure as that of the APFB homopolymer. It can be observed that the pp-APFB-PI (Ar) film obtained at the low RF power of 5 W has a *C*–H/*C*–CF/*C*F ratio of 3.0:1.1:3.7 (Fig. 1(a)). This ratio is closer to the theoretical ratio of 3:1:5 for the APFB homopolymer than those of the other films deposited at higher RF powers. Thus, the aromatic F of APFB can be preserved to a large extent (about 75 ± 10% based on the C 1s spectra line shape) for films deposited under the lower input RF power of 5 W. With the increase in input RF power, the APFB plasma contains more active species and radicals, which come from the excitation of the carbon–carbon π-bonds, as well as the scission of the C–H, C–C and C–F bonds. As a result, the extents of defluorination and molecular re-arrangement will increase with the increase in RF power. These reactions give rise to the decrease in intensity of the *C*–F component and the formation of more *C*F_2CH_2 species in the pp-APFB-PI (Ar) films. A weak component at the high BE of 291.8 eV, attributable to the *C*F_2CF_2 species, is also discernible in the spectrum of the film deposited at the RF power of 100 W [20].

The effects of the carrier gas and input RF power on the surface composition of the pp-APFB films are shown in Table 1. The [F]/[C] ratios of the pp-APFB films decrease with the increase in RF power for each of the four carrier gases used. This result suggests that the increase in RF power will give rise to more intensive defluorination of the pp-APFB films. The surface composition of the pp-APFB films varies significantly when different carrier gases are used. Among the four carrier gases used, argon gives rise to the highest, while O_2 gives rise to the lowest, [F]/[C] ratio at each input RF power level. The [F]/[C] ratios in Table 1 suggest that the extent of defluorination of the pp-APFB film with the carrier gas decreases in the following order: $O_2 > N_2 > H_2 >$ Ar. The data in Table 1 also show that the O_2 carrier gas gives rise to a high concentration of the oxygen-containing species in the pp-APFB film. The presence of N-containing species can only be observed in the pp-APFB film deposited using N_2 as the carrier gas. The nitrogen species with a BE at 398.4 eV were introduced by the N_2 plasma rather than arising from the nitrogen species in the underlying PI substrate. The N 1s peak component of the latter has a BE at about 400.6 eV [16]. Another interesting observation is that the [F]/[C] molar ratios of the pp-APFB-PI (Ar), pp-APFB-PI (H_2), and pp-APFB-PI (N_2) films deposited under the low RF power of 5 W are rather close to the theoretical ratio derived from the APFB structure. The latter has a [F]/[C] molar ratio of about 0.56. This result suggests that the fluorinated aromatic ring can be preserved to a high extent under the low RF power used in the present work.

3.2. Chemical structure of the plasma-polymerized APFB films (the pp-APFB films)

Comparison of the positive ion ToF-SIMS spectra of the pp-APFB-PI (Ar) films deposited at input RF power of 5 W (Fig. 2(a)) and 100 W (Fig. 2(b)) gives further support to the

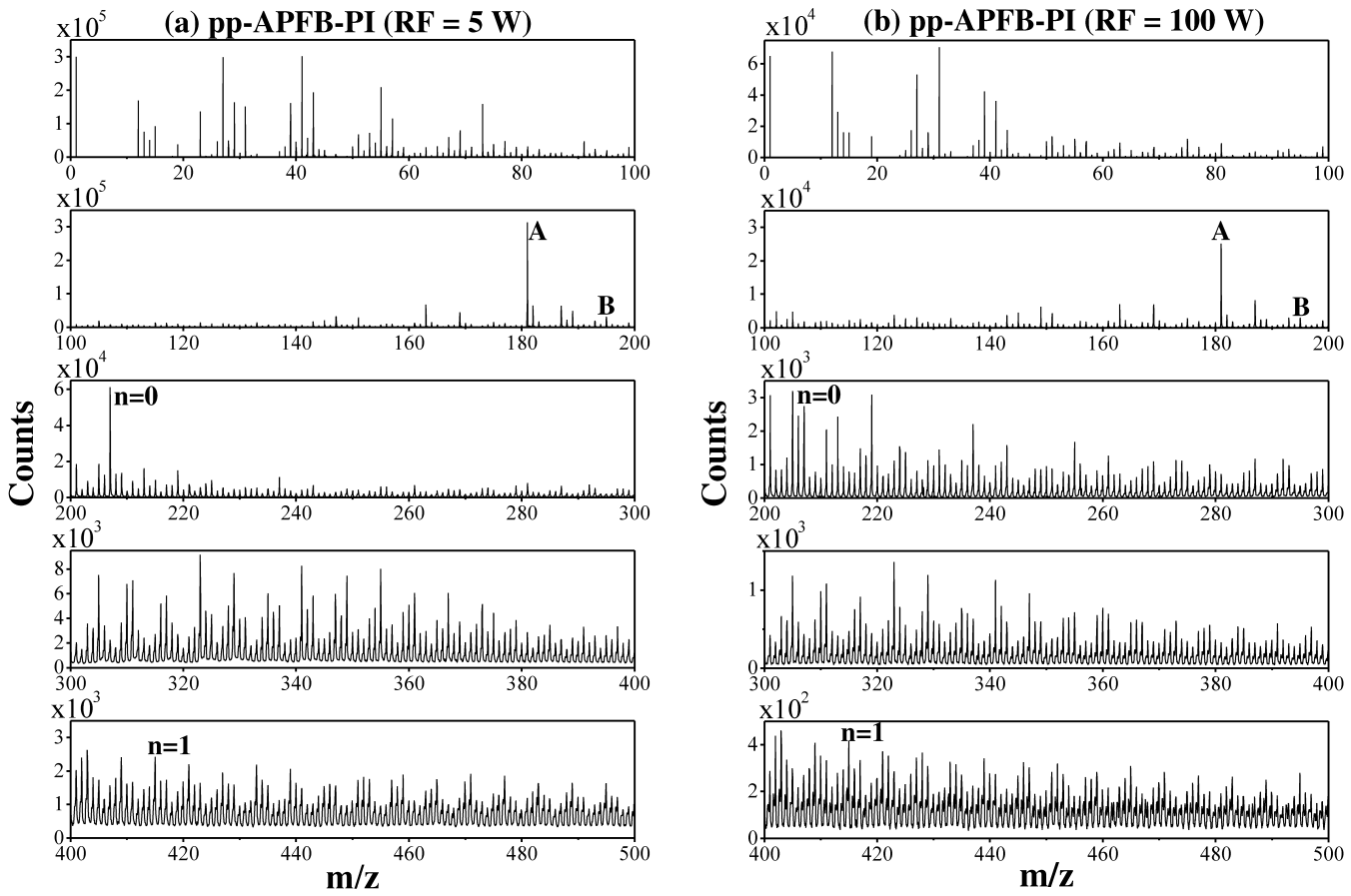

Fig. 2. Positive ion ToF-SIMS spectra of the pp-APFB-PI (Ar) films deposited at RF powers of (a) 5 W and (b) 100 W.

fact that a large proportion of the fluorinated aromatic ring can be preserved under the lower RF power. The assignment of the positive ions of the pp-APFB-PI (Ar) film is shown in Scheme 1.

The preservation of the fluorinated aromatic ring is readily indicated by the strong C_6F_5-CH_2 peak (peak A in Fig. 2) intensity and the presence of repeating units of the APFB monomer. In comparison with the peak intensities of the other fragments in the respective spectrum, the relative peak intensities of the APFB repeat units and the $C_6F_5-CH_2$ fragment of the pp-APFB-PI film deposited at 5 W are much higher than those of the corresponding fragments of the pp-APFB-PI film deposited at 100 W.

The chemical structure of the pp-APFB films was also studied by FTIR spectroscopy. Fig. 3 shows, respectively, the FTIR spectra of the APFB monomer (Fig. 3(a)) and the pp-APFB films (Fig. 3(b) to (i)) deposited on KBr pellets under the RF power of 5 W (Fig. 3(b), (d), (f) and (h)) and 70 W (Fig. 3(c), (e), (g) and (i)), using Ar (Fig. 3(b) and (c)), H_2 (Fig. 3(d) and (e)), N_2 (Fig. 3(f) and (g)), and O_2

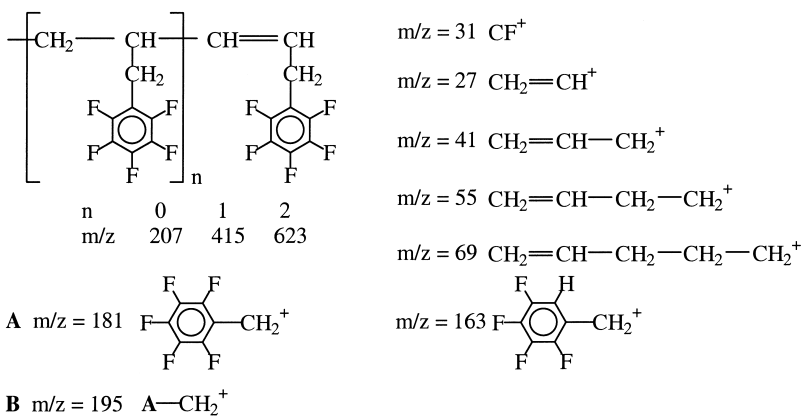

Scheme 1. Assignment of the positive ions in the ToF-SIMS spectra of the pp-APFB-PI surfaces.

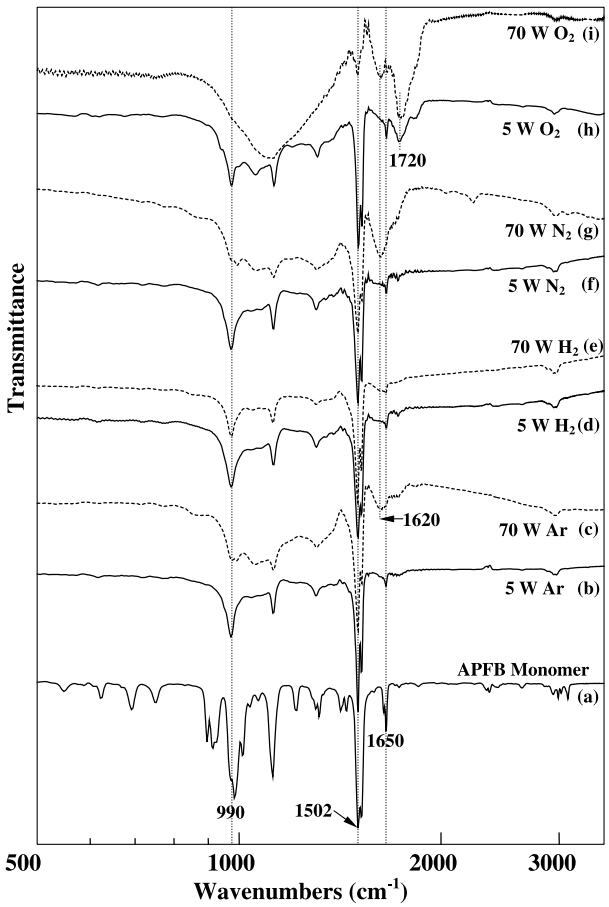

Fig. 3. FTIR spectra of (a) the APFB monomer, and the plasma-polymerized APFB (pp-APFB) films on KBr discs at RF powers of (b) 5 W and (c) 100 W using Ar-carried APFB; (d) 5 W and (e) 100 W using H_2-carried APFB; (f) 5 W and (g) 100 W using N_2-carried APFB; (h) 5 W and (i) 100 W using O_2-carried APFB.

(Fig. 3(h) and (i)) as the carrier gas. The FTIR spectrum of the APFB monomer displays the characteristic absorption bands of the aromatic C–F species at 990 cm^{-1} and of the fluorinated aromatic rings at 1502 cm^{-1} [10]. The absorption band at 1650 cm^{-1} is assigned to the stretching absorption of the C=C species.

In comparison to the APFB monomer spectrum in Fig. 3(a) and with the exception of the pp-APFB (O_2) films, the characteristic absorption band at 990 cm^{-1} for the aromatic C–F species has been preserved to a large extent for pp-APFB films deposited at 5 W (Fig. 3(b), (d) and (f)). On the other hand, however, the intensities of the corresponding absorption band in Fig. 3(c), (e), (g), and (i) for films deposited at 70 W have decreased substantially. The enhanced absorption at 1100–1300 cm^{-1} is observed in Fig. 3(c), (g), (h), and (i) and is due to the overlapping absorption of the CF_x species ($x = 1–3$). The presence of CF_x species in the pp-APFB films is consistent with the XPS result in Fig. 1. The enhanced absorption at 1100–1300 cm^{-1} in Fig. 3(h) and (i) is partially contributed by the absorption of the C–O–C species. The incorporation of oxygen into the pp-APFB-PI (O_2) films has been shown in Table 1. The incorporation of oxygen has also resulted in the formation of the C=O species, which has a characteristic absorption band at about 1720 cm^{-1} in Fig. 3(h) and (i), in the pp-APFB (O_2) film.

The FTIR results thus suggest that when glow discharge is carried out under the low RF power of 5 W, and using Ar, N_2, or H_2 as the carrier gas, the pp-APFB films are deposited via the dissociation of the π bonds in the APFB monomer. The cleavage of the C=C double bond in the plasma polymerization process can be deduced from the substantial decrease in the intensity of the absorption band at 1650 cm^{-1} for the pp-APFB films. An increase in RF power or the use of O_2 as the carrier gas will lead to an increase in the extent of defluorination, and thus the degree of complexity, of the aromatic structure in the resulting pp-APFB film. As a result, the lineshape of the aromatic absorption band at 1502 cm^{-1} is altered. The presence of aromatic rings with reduced degree of fluorination is also indicated by the appearance of the absorption band at about 1620 cm^{-1} [22] as indicated in Fig. 3(c), (e), (g), and (i).

Different carrier gases also give rise to pp-APFB films of different structures. The O_2 gas leads to the most drastic changes in structure of the deposited pp-APFB film. Even under the low input RF power, the O_2 plasma can result in extensive defluorination of the aromatic rings and the incorporation of oxygen-containing groups. By taking into consideration the XPS results in Table 1, the extent of defluorination during plasma polymerization by the four carrier gases decreases in the following order: $O_2 > N_2 > H_2 > Ar$. This result appears to differ from the strong defluorination ability of the H_2 plasma during the gas plasma treatment of the fluoropolymer substrates [23].

3.3. Surface topography of the pp-APFB-PI films

Surface topography is of great importance to the surface wettability of the polymer films [24]. Fig. 4(a)–(h) shows the AFM images of the pp-APFB layer deposited on PI films under the RF power of 5 W (Fig. 4(a), (c), (e) and (g)) and 100 W (Fig. 4(b), (d), (f) and (h)), using Ar (Fig. 4(a) and (b)), H_2 (Fig. 4(c) and (d)), N_2 (Fig. 4(e) and (f)), and O_2 (Fig. 4(g) and (h)) as the carrier gas. The deposition time for all the samples is 40 s. Previous studies have reported that the average surface roughness value, R_a, of the pristine PI (Kapton® HN) film surface is about 1.5 nm [25,26]. Under the low input RF power of 5 W, plasma polymerization and deposition of APFB using any one of the four carrier gases can give rise to a very uniform surface. The R_a value of the pp-APFB-PI film surface deposited at 5 W using argon as the carrier gas increases to about 3.5 nm. The other carrier gases, viz., H_2, N_2, and O_2, however, give rise to an even smoother surface. The R_a values decrease to 0.7, 1.2, and 0.7, respectively. On the other hand, however, for plasma polymerization carried out under the high RF power of 100 W, the surface roughness of the pp-APFB-PI film increases significantly. The R_a value of the pp-APFB-PI

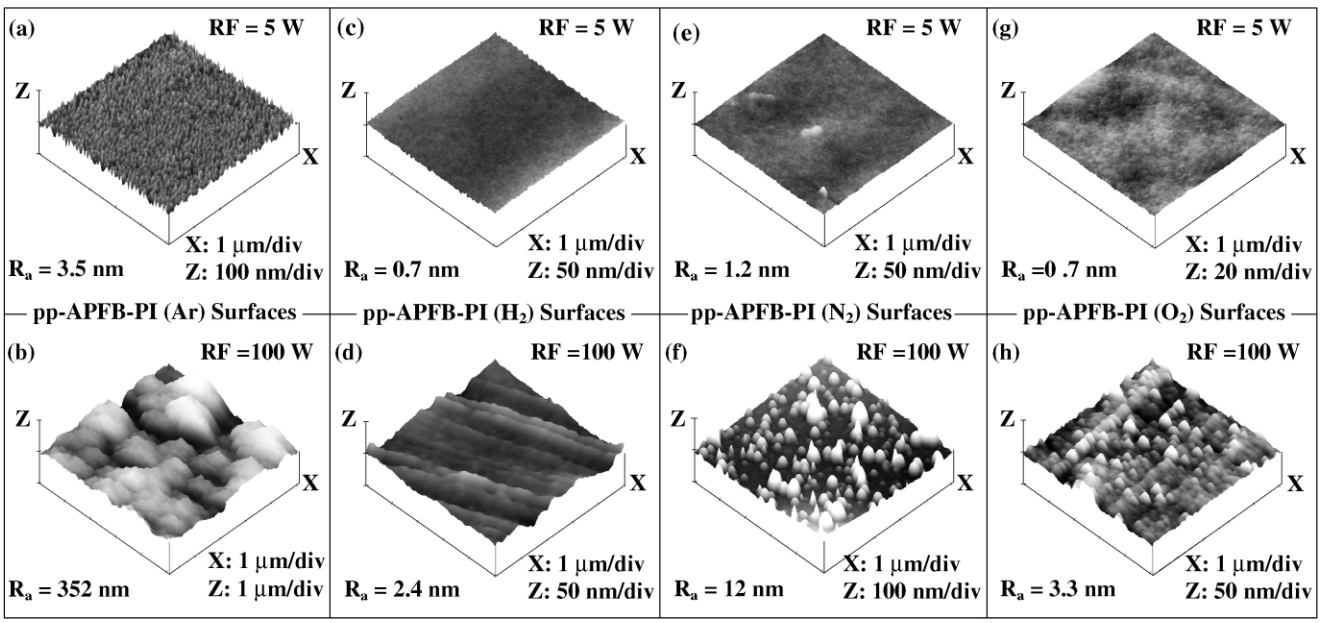

Fig. 4. AFM images of the pp-APFB-PI surfaces obtained at RF powers of (a) 5 W and (b) 100 W using Ar-carried APFB; (c) 5 W and (d) 100 W using H_2-carried APFB; (e) 5 W and (f) 100 W using N_2-carried APFB; (g) 5 W and (h) 100 W using O_2-carried APFB.

(Ar) film deposited under the RF power of 100 W is about 300 times that of the pristine PI surface. Earlier studies [16,17] have shown that a high input RF power will generate more excited species in the plasma chamber. The excited species, in turn, give rise to the formation of more crosslinked aggregates on the PI surface and account for the observed increase in high surface roughness.

3.4. Surface wettability of the pp-APFB-PI films

Table 2 shows the advancing (θ_A) and receding (θ_R) water contact angles of the pp-APFB-PI films obtained under different RF powers using argon as the carrier gas. For comparison purposes, the water contact angles of the pristine PI (Kapton® HN), FPI (Kapton® FN), and PTFE films are also shown in Table 2. It can be observed that the pp-APFB-PI (Ar) surface is much more hydrophobic than the pristine PI and FPI surface. Under the high input RF power, the advancing and receding water contact angles of the pp-APFB-PI (Ar) surface are much larger than those of the pristine PTFE surface. The advancing water contact angle reaches as high as 174°, which is about 60° higher than that of the PTFE surface and 3 times that of the pristine PI surface. The hysteresis effect of the water contact angle on the pp-APFB-PI (Ar) surface is probably due to incorporation of some oxygen-containing species in the pp-APFB film after exposure to air. The presence of incorporated oxygen species is indicated by the surface composition data in Table 1. The ultra-hydrophobic nature of the pp-APFB-PI (Ar) surface is also revealed by the contour of the contacting water droplet. Fig. 5 shows the optical images of the water droplet on the pp-APFB-PI (Ar) surface with an advancing contact angle of 174° (Fig. 5(a)) and a receding contact angle of 140° (Fig. 5(b)). It is appropriate to point out that although the terms ultra-hydrophobic or super-hydrophobic surface have been suggested in the earlier work of Youngblood and McCarthy [27] for surfaces showing little or no hysteresis in advancing and receding contact angles, the term ultra-hydrophobic surface is used in the present work merely to indicate the fact that the pp-APFB-PI (Ar) surface is substantially more hydrophobic than the PTFE surface.

Plasma polymerization parameters affect the surface composition and topography, and thus the surface wettability, of the deposited polymer films. Fig. 6 shows the dependence of the static water contact angle of the pp-APFB-PI surface on the input RF power and the type of carrier gas used. The water contact angle of the corresponding surface after thorough washing in methyl ethyl ketone is also plotted in Fig. 6 for comparison purpose. The samples were annealed at 250 °C for 2 h under vacuum prior to solvent extraction. The water contact angle of the pp-APFB-PI (Ar) surface increases with the input RF power. On the

Table 2
Advancing (θ_A) and receding (θ_R) water contact angle of different polymer surfaces

Surfaces	θ_A (°)	θ_R (°)
PTFE film	111 ± 1	77 ± 2
PI Film (Kapton® HN)	53 ± 2	31 ± 5
FPI film (Kapton® FN)	71 ± 1	37 ± 2
pp-APFB-PI (Ar)[a]	84 ± 3	52 ± 1
pp-APFB-PI (Ar)[b]	174 ± 2	135 ± 7

[a] Deposition conditions: RF power = 5 W.
[b] Deposition conditions: RF power = 100 W.

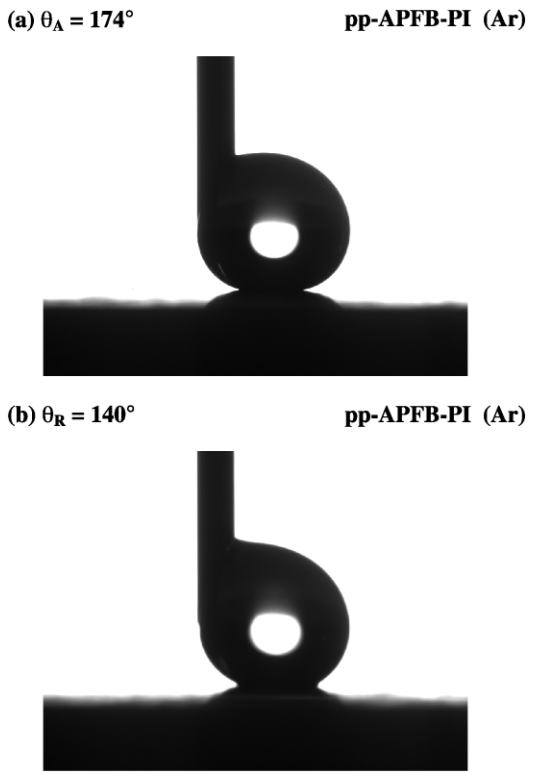

Fig. 5. Optical images of a water droplet on a pp-APFB-PI (Ar) surface with advancing and receding water contact angles of (a) $\theta_A = 174°$ and (b) $\theta_R = 140°$.

other hand, the water contact angles of the other three types of pp-APFB-PI surfaces prepared using H_2, N_2, or O_2 as the carrier gas, decrease slightly with the input RF power. Since the water contact angle is related to the synergetic effects of surface chemistry and surface topography, the results in Fig. 6 can be attributed to the following factors. The increase in RF power will give rise to a change in surface composition of the pp-APFB-PI film. The decrease in the [F]/[C] ratio (and thus the decrease in hydrophobicity due to defluorination) of the pp-APFB-PI surface with the input RF power is shown in Table 1. The incorporation of oxygen and nitrogen-containing groups will result in the further loss in surface hydrophobicity of the pp-APFB layer. On the other hand, the increase in RF power will give rise to an increase in the surface roughness. According to Wenzel's equation [24], the increase in surface roughness will give rise to a larger water contact angle (θ) for a hydrophobic surface (with $\theta > 90°$) and a lower water contact angle for a hydrophilic surface (with $\theta < 90°$). Table 1 shows that the fluorine concentration (the [F]/[C] ratio) of the pp-APFB-PI (Ar) surface decreases only slightly, from 0.53 to 0.50, when the RF power is increased from 5 to 150 W. Furthermore, the [O]/[C] ratios for all the five surfaces deposited using Ar as the carrier gas remains relatively low. These results suggest that the hydrophobic fluorinated species are preserved, to a large extent, on all the pp-APFB-PI (Ar) surfaces. Finally, the AFM image in Fig. 4(b) reveals that the average surface roughness, R_a, of the pp-APFB-PI (Ar)

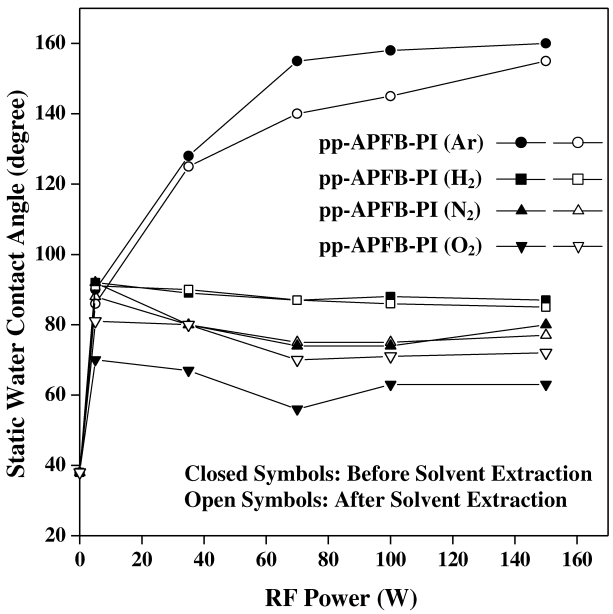

Fig. 6. Effect of the input RF power and the type of the carrier gas on the static water contact angle of the pp-APFB-PI surfaces.

film deposited at 100 W is substantially higher than that of the pristine PI surface. Thus, the large water contact angle observed for the pp-APFB-PI (Ar) surface probably has resulted from the synergistic effect of the preservation of the hydrophobic species and the marked increase in surface roughness.

In contrast to the pp-APFB-PI (Ar) film, the films prepared using the other three carrier gases exhibit a decrease in water contact angle with the increase in RF power. This phenomenon is attributed to the loss of surface hydrophobicity due to defluorination and the incorporation of hydrophilic O- and N-containing species into the deposited pp-APFB films. The increase in surface roughness of these films, on the other hand, will give rise to the further decrease in water contact angle, according to Wenzel's equation, especially for pp-APFB surfaces with contact angles below 90°. It can also be observed that the water contact angles for the pp-APFB-PI (O_2) and the pp-APFB-PI (N_2) surfaces drop below 80° at the RF power of about 70 W.

The data in Fig. 6 also indicate that, except for the pp-APFB-PI (O_2) films, the water contact angles of the pp-APFB-PI films after solvent extraction remained almost unchanged. This result suggests that the pp-APFB films are chemical resistant. The substantial increase in water contact angle of the pp-APFB-PI (O_2) surface after solvent extraction is probably due to both the decomposition of the hydrophilic species during thermal annealing and the removal of the oxygen-containing species by the solvent. The removal of the oxygen-containing species is further confirmed by the substantial decrease in the [O]/[C] ratio of the surface after solvent extraction. In contrast to the effect of carrier gas on defluorination, the effect of the carrier gas

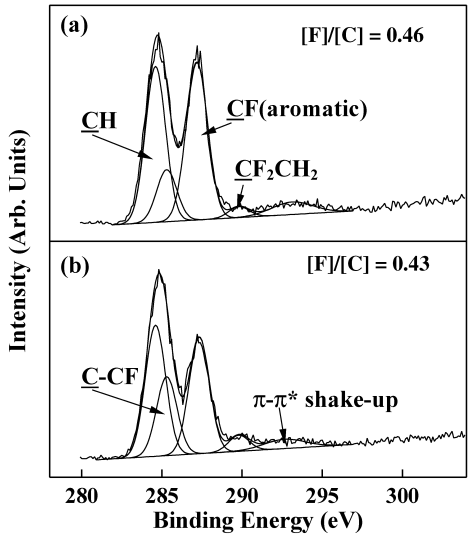

Fig. 7. C 1s core-level spectra of the pp-APFB-PI (Ar) surfaces from input RF powers of (a) 5 W and (b) 70 W after thermal annealing and solvent extraction.

on the surface hydrophobicity of the pp-APFB-PI film increases in the order of $O_2 < N_2 < H_2 < Ar$. Thus, the increase in water contact angle of the pp-APFB-PI surface coincides with the increase in surface fluorine concentration. Minimizing defluorination during plasma polymerization and deposition will help to improve the surface hydrophobicity. In this respect, the present study supplements the earlier studies on the liquid repellent plasma films [9–13] by elucidating the effects of plasma power and type of carrier gas on the surface topography and chemical composition of the deposited films. The latter two parameters, in turn, have a significant bearing on the observed surface hydrophobicity.

3.5. Interaction of pp-APFB with the PI substrate

The interaction between the pp-APFB film and the Ar plasma-pretreated PI substrate was evaluated by two consecutive processes. Initially, the pp-APFB-PI (Ar) film was annealed in a vacuum oven for 2 h at 250 °C and then immersed in methyl ethyl ketone solution for 6 h. The thermally annealed and solvent-extracted pp-APFB-PI film was adhered to a Scotch® tape. The Scotch® tape was subsequently peeled off from the pp-APFB-PI film. After three adhere-and-peel cycles using the same piece of tape, the delaminated surfaces were analysed by XPS.

Fig. 7(a) and (b) shows the respective C 1s core-level spectra of the pp-APFB-PI (Ar) films, prepared at the RF powers of 5 and 70 W, after thermal annealing and solvent extraction. The corresponding spectra of the as-deposited pp-APFB-PI (Ar) have been shown, respectively, in Fig. 1(a) and (c). In comparison with the C 1s spectra of the as-deposited surfaces, the intensities of the corresponding *C*F (aromatic) peak components in Fig. 7(a) and (b) have decreased slightly after the solvent extraction. The [F]/[C]

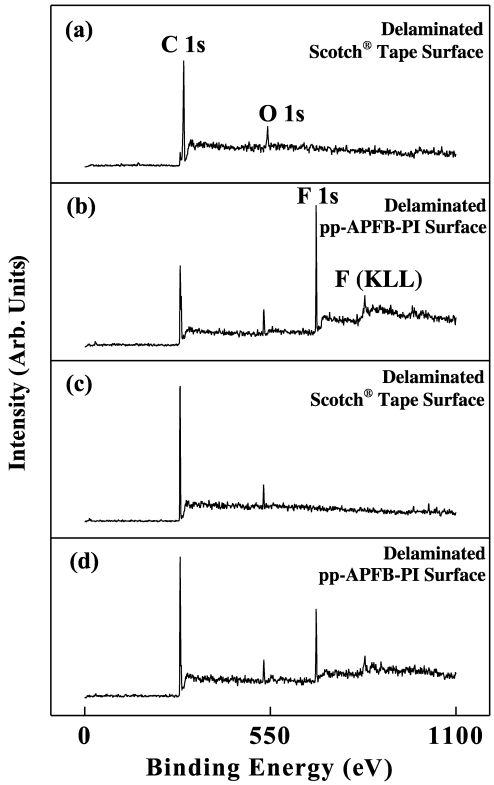

Fig. 8. XPS wide scan spectra of the delaminated (a) Scotch® tape and (b) PI surfaces from a Scotch® tape/pp-APFB-PI (Ar) assembly, with the pp-APFB deposited at 5 W, and the delaminated (c) Scotch® tape and (d) PI surfaces from a Scotch® tape/pp-APFB-PI (Ar) assembly, with the pp-APFB deposited at 70 W.

ratios of the pp-APFB-PI (Ar) surfaces prepared at the two RF powers decrease from about 0.53 and 0.50 (before solvent extraction) to about 0.46 and 0.43 (after solvent extraction), respectively. These results suggest that a small amount of low molecular weight species, which contains more fluorinated aromatic rings, has been removed during the solvent extraction process. However, the persistent of strong intensities for the *C*F (aromatic) peak component and the shake-up satellite in the C 1s spectra of the two extracted pp-APFB-PI (Ar) surfaces suggests that the pp-APFB layer is strongly tethered on the Ar plasma-pretreated PI substrate. In spite of the removal of the low molecular weight species, the thickness of the pp-APFB layers did not change appreciably, especially for the layer deposited at the high RF power. This result suggests the presence of a more porous microstructure for the pp-APFB layers after the thermal treatment and solvent extraction.

Fig. 8 shows the wide scan spectra of the surfaces of Scotch® tape peeled off from a 5-W (Fig. 8(a)) and a 70-W pp-APFB-PI (Ar) surface (Fig. 8(c)). The corresponding wide scan spectra of the delaminated PI surfaces are shown, respectively, in Fig. 8(b) and (d). The 180°-peel adhesion strength of the Scotch® tape on the pp-APFB-PI surfaces was in the order of 2 N/cm. The fact that no fluorine signal is discernible in the wide scan spectra of the delaminated Scotch® tape surfaces, together with the persistence of the

strong fluorine signals and the appearance of a fairly strong O 1s signal (from the adhesive residue of the tape) in the wide scan of the delaminated PI surfaces, give further support to the fact that the pp-APFB layers are strongly bonded to the PI surfaces.

4. Conclusion

Allylpentafluorobenzene (APFB) was plasma-polymerized and deposited on the plasma-pretreated PI film surfaces. The effects of the carrier gas (Ar, H_2, N_2 and O_2) and the input RF power on surface composition and topography of the deposited APFB polymer films were studied. XPS, FTIR, and ToF-SIMS results revealed that the fluorinated aromatic ring of the plasma-deposited APFB polymer (pp-APFB) could be retained, to a large extent, under proper glow discharge conditions, such as a low input RF power of 5 W, and the use of non-reactive argon as the carrier gas. The preservation of the fluorinated species in the pp-APFB-PI surface, especially for pp-APFB layer deposited using argon as the carrier gas, and the substantial increase in surface roughness had given rise to an ultrahydrophobic surface with large advancing and receding water contact angles (θ_A/θ_R) of 174°/135°. The effectiveness of the carrier gas in defluorination during the deposition of the pp-APFB film decreased in the order of $O_2 > N_2 > H_2 > Ar$. The effectiveness of the carrier gas in improving surface hydrophobicity of the pp-APFB-PI film, on the other hand, increased in the order of $O_2 < N_2 < H_2 < Ar$. Solvent extraction and Scotch® tape peel test revealed that the pp-APFB layer was strongly bonded to the PI film surface. Thus, plasma polymerization of fluorine-containing monomers provides an alternative approach to the deposition of hydrophobic barriers and passivating thin films.

References

[1] Maier G. Prog Polym Sci 2001;26:3.
[2] Kreuz JA, Edman JR. Adv Mater 1998;10:1229.
[3] Brandrup J, Immergut EH. Polymer handbook, 3rd ed. New York: Wiley; 1989. p. V/1.
[4] Sasaki S, Nishi S. In: Ghosh MK, Mittal KL, editors. Polyimides: fundamentals and applications. New York: Marcel Dekker; 1996. p. 71.
[5] Endo K, Tatsumi T. J Vac Sci Technol A 1997;15:3134.
[6] Yasuda T, Okuno T, Miyama M, Yasuda H. J Polym Sci Polym Chem 1994;32:1829.
[7] Matienzo LJ, Emmi F, Egitto FD, Van Hart DC, Vukanovic V, Takacs GA. J Vac Sci Technol A 1988;6:950.
[8] Kang ET, Zhang Y. Adv Mater 2000;12:1481.
[9] Han LCM, Timmons RB, Lee WW. J Vac Sci Technol B 2000;18:799.
[10] Han LCM, Timmons RB, Lee WW, Chen YY, Hu ZB. J Appl Phys 1998;84:439.
[11] Coulson SR, Woodward IS, Badyal JPS, Brewer SA, Willis C. Langmuir 2000;16:6287.
[12] Coulson SR, Woodward IS, Badyal JPS, Brewer SA, Willis C. Chem Mater 2000;12:2031.
[13] Chen W, Fadeev AY, Hsieh MC, Oner D, Youngblood J, McCarthy TJ. Langmuir 1999;15:3395.
[14] Yang GH, Kang ET, Neoh KG. J Polym Sci Part A: Polym Chem 2000;38:3498.
[15] Zhang Y, Tan KL, Yang GH, Zou XP, Kang ET. J Adhes Sci Technol 2000;14:1723.
[16] Zhang Y, Tan KL, Liaw BY, Liaw DJ, Kang ET, Neoh KG. Langmuir 2001;17:2265.
[17] Yasuda H, Hirotsu T. J Polym Sci Polym Chem Ed 1978;16:743.
[18] Inagaki N. Plasma surface modification and plasma polymerization. Lancaster, PA: Technomic; 1996. Chapter 5.
[19] Tan KL, Woon LL, Kang ET, Neoh KG. Macromolecules 1993;26:2832.
[20] Muilenberg GE. Handbook of X-ray photoelectron spectroscopy. Eden Prairie, MN: Perkin–Elmer; 1978. p. 38.
[21] Huheey JE. Inorganic chemistry, 2nd ed. New York: Harper & Row; 1978. Appendix F.
[22] Pouchert CJ, 1st ed. The Aldrich library of FT-IR spectra, Vol. 1. Milwaukee, WI: Aldrich Chem. Co; 1985. p. 1010.
[23] Shi MK, Martinu L, Secher E, Selmani A, Wertheimer MR, Yelon A. Surf Interface Anal 1995;23:99.
[24] Wenzel RN. Ind Engng Chem 1936;28:988.
[25] Yang GH, Kang ET, Neoh KG, Zhang Y, Tan KL. Colloid Polym Sci 2001;279:745.
[26] Zhang Y, Tan KL, Yang GH, Kang ET, Neoh KG. J Electrochem Soc 2001;148:C574.
[27] Youngblood JP, McCarthy TJ. Macromolecules 1999;32:6800.